# Influence of Geometric Parameters of the Hydrocyclone and Sand Concentration on the Water/Sand/Heavy-Oil Separation Process: Modeling and Simulation

**F.P.M. Farias[1], J.S. Souza[2], W.C.P.B. de Lima[2], A.C. de Macêdo[2], S.R. de Farias Neto[3], A.G.B. de Lima[2]**

[1,2,3]Federal University of Campina Grande (UFCG)
Center for Sustainable Development of the Semi-Arid (CDSA)
[1]Department of Technology and Development,
Av. Luiz Grande - Zip Code 58540-000, Sumé, Paraíba, Brazil.
Center of Science and Technology (CCT)
[2]Department of Mechanical Engineering
[3]Department of Chemical Engineering
Av. Aprígio Veloso, 882- Bodocongó - ZIP Code 58429-900,
Campina Grande, Paraíba, Brazil

**ABSTRACT**

In the oil exploitation, produced fluids are composed of oil, gas, water and sand (depending on the reservoir location). The presence of sand in flow oil leads to several industrial problems for example: erosion and accumulation in valves and pipeline. Thus, it is necessary to stop production for manual cleaning of equipments and pipes. These facts have attracted attention of academic and industrial areas, enabling the appearing of new technologies or improvement of the water/oil/sand separation process. One equipment that has been used to promote phase separation is the hydrocyclone due to high performance of separation and required low cost to installation and maintenance. In this sense, the purpose of this work is to study numerically the effect of geometric parameters (vortex finder diameter) of the hydrocyclone and sand concentration on the inlet fluid separation process. A numerical solution of the governing equations was obtained by the ANSYS CFX-11 commercial code. Results of the streamlines, pressure drop and separation efficiency on the hydrocyclone are presented and analyzed. It was observed that the particles concentration and geometry affect the separation efficiency of the hydrocyclone.

**Keywords:** Hydrocyclone; Droplet size; Heavy-oil; Computational Fluid Dynamics

## 1. INTRODUCTION

Produced water can be defined as any water that is present in a reservoir of the hydrocarbon reserve. During the production phase water flows together with the crude oil or natural gas to the surface. The composition of this water usually includes a mixture of liquid or gaseous hydrocarbons, dissolved solids (carbonates, sulfates, sodium chloride, potassium chloride, calcium chloride and magnesium chloride) and suspended solids (sand, silt, clay, gypsum,

etc). Dispersed oil can be considered as an important pollutant, because of toxic effects in the vicinity of the discharge area. The concentration of this contaminant depends on different factors, such as: oil density, interfacial tension between oil and water phases, type and efficiency of chemical treatment, and type, size, and efficiency of the physical separation equipment. Solids produced can contain carbonates, clays, corrosion products and others precipitated or suspended solids resultant of oilfields. These solids can influence the efficiency of oil-water separators and sometimes can form oily sludges in production equipment thus a periodic maintenance is required.

The presence of produced solids, even at low flow rates causes problems in the production system such as erosion in valves and pipelines, causing an increase in pumping power [1]. For minimize the problems caused by produced solids and to clean the produced water, it is necessary to promote the phase separation. An example of equipment for this separation is a hydrocyclone. This equipment is largely used in oilfields (offshore and onshore) for produced water treatment [2]. Hydrocyclones are attractive for industrial use because they offer significant advantages such as significant reduction in equipment dimensions, no moving parts, relatively low capital and operating costs, easy to operate, short residence time and high centrifugal forces generated [3,4].

Several studies have been reported in the literature related to the separation process using hydrocyclones: Cullivan *et al*. [5]; Petty and Parks [6]; Simões [7]; Brennan *et al*. [8]; Delgadillo and Rajamani [9]; Sripriya e*t al*. [10]; Zhao *et al*. [11]; Farias *et al*. [12]; Martínez *et al*. [13]; Mousavian and Najafi [14]; Wang and Yu [15]; Buriti [16].

In accordance with Kraipech *et al*. [17], the hydrodynamic behavior of hydrocyclones used to treat concentrated slurries, in special the produced waters and produced solids, have yet to be fully understood. In this sense, the purpose of the present work is to study the influence of hydrocyclone overflow diameter and solid (sand) concentration in the inlet section on the water/sand/heavy-oil separation process.

## 2. MODEL DESCRIPTION

### 2.1. MATHEMATICAL MODEL

The mathematical modelling to describe the multiphase fluid flow inside the hydrocyclone is constituted by two sets of conservation equations: balance of mass and momentum for each of the phases [18]. The hydrocyclone has been assumed to be operating at steady state conditions where the classical equations of fluid dynamics can be applied. So, the continuity and momentum equations were used to determine the multiphase flow field.

#### *2.1.1. Continuity equation*

The mass conservation equation is given by:

$$\frac{\partial}{\partial t}\left(f_\alpha \rho_\alpha\right) + \nabla \cdot \left(f_\alpha \rho_\alpha \mathbf{U}_\alpha\right) = \sum_{\beta=1}^{N_p} \Gamma_{\alpha\beta} + \mathbf{S}_{MS\alpha} \tag{1}$$

where the subscript $\alpha$ represent the phases involved (water, heavy oil and sand); $f$ is the volume fraction; $\rho$ is density and $\mathbf{U}$ is the velocity vector; $\mathbf{S}_{M\alpha}$ describes user specified mass sources, and $\Gamma_{\alpha\beta}$ is the mass flow rate per unit volume from phase $\alpha$ to phase $\beta$. This term only occurs if interphase mass transfer takes place. For details see ANSYS CFX [18].

### 2.1.2. Momentum equation

The momentum conservation equation is given by:

$$\frac{\partial}{\partial t}\left(f_\alpha \rho_\alpha \mathbf{U}_\alpha\right) + \nabla \cdot \left[f_\alpha\left(\rho_\alpha \mathbf{U}_\alpha \otimes \mathbf{U}_\alpha\right)\right] = -f_\alpha \nabla p_\alpha + \nabla \cdot \left\{f_\alpha \mu_\alpha \left[\nabla \mathbf{U}_\alpha + \left(\nabla \mathbf{U}_\alpha\right)^T\right]\right\} + \sum_{\beta=1}^{N_P}\left(\Gamma_{\alpha\beta}\mathbf{U}_\beta - \Gamma_{\beta\alpha}\mathbf{U}_\alpha\right) + \mathbf{S}_\alpha + \mathbf{M}_\alpha \tag{2}$$

where $\mu$ is dynamic viscosity; $p_\alpha$ is the pressure; $\mathbf{S}_\alpha$ describes momentum sources due to external body (buoyancy force and rotational force); the term ($\Gamma_{\alpha\beta}\mathbf{U}_\beta - \Gamma_{\beta\alpha}\mathbf{U}_\alpha$) represents momentum transfer induced by interphase mass transfer and occurs when mass is carried from one phase into another; $\Gamma_{\beta\alpha}$ is a positive mass flow rate per unit volume from phase $\beta$ to phase $\alpha$ and $\mathbf{M}_\alpha$ describes the total force on phase $\alpha$ due to interaction with other phases, such as drag force, lift force, virtual mass force, etc. This term is given by:

$$\mathbf{M}_\alpha = \mathbf{M}^D_{\alpha\beta} + \mathbf{M}^L_{\alpha\beta} + \mathbf{M}^{LUB}_{\alpha\beta} + \mathbf{M}^{VM}_{\alpha\beta} + \mathbf{M}^{TD}_{\alpha\beta} + \mathbf{M}_S \tag{3}$$

where $\mathbf{M}^D_{\alpha\beta},, \mathbf{M}^L_{\alpha\beta}, \mathbf{M}^{LUB}_{\alpha\beta}, \mathbf{M}^{VM}_{\alpha\beta}, \mathbf{M}^{TD}_{\alpha\beta}$ and $\mathbf{M}_S$ represent the drag force, lift force, wall lubrication force, virtual mass force, turbulence dispersion force and solids pressure force (for dense solid particle phases only), respectively. In this work, $\mathbf{M}^L_{\alpha\beta}, \mathbf{M}^{LUB}_{\alpha\beta}, \mathbf{M}^{VM}_{\alpha\beta}$ *and* $\mathbf{M}^{TD}_{\alpha\beta}$ were neglected. The interphase drag force, $\mathbf{M}^D_{\alpha\beta}$, acts in the direction opposing the relative flow between the phases. It is defined by the following equation:

$$\mathbf{M}^D_{\alpha\beta} = \frac{C_D}{8}\rho_\alpha A_{\alpha\beta}\left|\mathbf{U}_\beta - \mathbf{U}_\alpha\right|\left(\mathbf{U}_\beta - \mathbf{U}_\alpha\right) \tag{4}$$

where $\alpha$ and $\beta$ represent the continuous phase and dispersed phase, respectively. The term $A_{\alpha\beta}$ correspond to the interfacial area density, which is characterized by the interfacial area per unit volume between the phases $\alpha$ and $\beta$. It is given by:

$$A_{\alpha\beta} = \frac{6 f_\beta}{d_\beta} \tag{5}$$

where $d_\beta$ is the mean diameter of spherical particles, $f_\beta$ is the volume fraction of dispersed phase and $C_D$ = 0.44, is the drag coefficient.

### 2.1.3. The SSG Reynolds Stress Model

The movement of the fluid and solid particles within the hydrocyclone is very complex and turbulent. So, to describe the multiphase flow inside the hydrocyclone correctly, it is necessary to use an appropriate turbulent model.

The standard Reynolds stress model in ANSYS CFX is based on the turbulence eddy dissipation equation. The ANSYS CFX use the following equations for this model:

$$\frac{\partial\left(\rho\overline{\mathbf{u}\otimes\mathbf{u}}\right)}{\partial t} + \nabla\cdot\left(\rho\mathbf{U}\otimes\overline{\mathbf{u}\otimes\mathbf{u}}\right) = \left\{\mathbf{P} + \phi + \nabla\cdot\left[\left(\mu + \frac{2}{3}c_S\rho\frac{k^2}{\varepsilon}\right)\nabla\otimes\overline{\mathbf{u}\otimes\mathbf{u}}\right] - \frac{2}{3}\rho\varepsilon\delta\right\} \tag{6}$$

where **U** is the velocity divided into an average component, $U_{med}$, and a time varying component, **u**, (**U** = $U_{med}$ + **u**), $\phi$ is the pressure-strain tensor, $\varepsilon$ is the turbulence eddy dissipation, $k$ is the turbulent kinetic energy, $c_S$ is the Reynolds stress model constant, $\delta$ is the identity matrix and **P** is the production term given by:

$$\mathbf{P} = -\rho\left[\left(\overline{\mathbf{u}\otimes\mathbf{u}}(\nabla\mathbf{U})^T + (\nabla\mathbf{U})\overline{\mathbf{u}\otimes\mathbf{u}}\right)\right] \tag{7}$$

When turbulence dissipation appears in the individual stress equations, an equation for $\varepsilon$ is still required. It has now the form:

$$\frac{\partial(\rho\varepsilon)}{\partial t} + \nabla(\rho\mathbf{U}\varepsilon) = \frac{\varepsilon}{k}\left(C_{\varepsilon_1}\mathbf{P} - C_{\varepsilon_2}\rho\varepsilon\right) + \nabla\cdot\left[\frac{1}{\sigma_{\varepsilon RS}}\left(\mu + \rho C_{\mu RS}\frac{k}{\varepsilon}\right)\nabla\cdot\varepsilon\right] \tag{8}$$

where $C_{\varepsilon_1}$, $C_{\varepsilon_2}$, $C_{\mu RS}$ and $\sigma_{\varepsilon RS}$ are Reynolds stress model constants.

One of the most important terms in the Reynolds stress model is the pressure-strain correlation, $\phi$. The pressure-strain correlations can be expressed in the general form as follows:

$$\phi = \phi_1 + \phi_2 \tag{9}$$

where:

$$\phi_1 = \rho\varepsilon\left[C_{S_1}\mathbf{a} + C_{S_2}\left(\mathbf{a}\mathbf{a} - \frac{1}{3}\mathbf{a}\cdot\mathbf{a}\delta\right)\right] \tag{10}$$

$$\begin{aligned}\phi_2 = &- C_{r_1}\mathbf{P}\mathbf{a} + C_{r_2}\rho k\mathbf{S} - C_{r_3}\rho k\mathbf{S}\sqrt{\mathbf{a}\cdot\mathbf{a}} + C_{r_4}\rho k\left(\mathbf{a}\mathbf{S}^T + \mathbf{S}\mathbf{a}^T - \frac{2}{3}\mathbf{a}\cdot\mathbf{S}\delta\right)\\ &+ C_{r_5}\rho k\left(\mathbf{a}\mathbf{W}^T + \mathbf{W}\mathbf{a}^T\right)\end{aligned} \tag{11}$$

where $C_{r_1}, C_{r_2}, C_{r_3}, C_{r_4}, C_{r_5}$ are constants of the model and,

$$\mathbf{a} = \frac{\overline{\mathbf{u}\otimes\mathbf{u}}}{k} - \frac{2}{3}\delta \tag{12}$$

$$\mathbf{S} = -\frac{1}{2}\left[\nabla\mathbf{U} + \left(\nabla\mathbf{U}^T\right)\right] \tag{13}$$

$$\mathbf{W} = \frac{1}{2}\left[\nabla\mathbf{U} - \left(\nabla\mathbf{U}^T\right)\right] \tag{14}$$

In equations 10, 11 and 12, **a** is the anisotropy tensor, **S** is the strain rate and **W** is the vorticity. This general form can be used to model linear and quadratic correlations by using appropriate values for the constants.

The SSG Reynolds stress model uses a quadratic relation for the pressure-strain correlation. The constants of this model are:

$$C_{\mu RS} = 0.1;\ C_{\varepsilon_1} = 1.45;\ C_{\varepsilon_2} = 1.83;\cdot\sigma_{\varepsilon RS} = 1.36;\ C_{s_1} = 1.7;\ C_{s_2} = -1.05;\ c_s = 0.22$$

$$C_{r_1} = 0.9; C_{r_2} = 0.8; C_{r_3} = 0.65; C_{r_4} = 0.625; C_{r_5} = 0.2$$

### *2.1.4. Solid Pressure Force Model*

The solid pressure force model is available for dispersed solid phases in a multiphase flow. The forces due to solid collisions are taken into account by introducing additional solids pressure and solids stress terms into the solid phase momentum equation based on either the Gidaspow model or by specifying the elasticity modulus directly. The constitutive model proposed by Gidaspow is given by:

$$\nabla P_S = G\left(g_S\right) + \nabla g_S \tag{15}$$

where $G(g_S)$ is the elasticity modulus, given by:

$$G\left(g_S\right) = + G_0 e^{c\left(g_S - g_{S,\max}\right)} \tag{16}$$

where $G_0$ is the reference elasticity modulus, $c$ is the compaction modulus, and $g_{S,\max}$ is the maximum packing parameter. The values of these variables are:

$$G_0 = 0.376 \text{ (Pa)};\ c = 600;\ g_{S,\max} = 0.62$$

Additional theoretical information on these models is available in ANSYS CFX® [18].

## 2.2. DESCRIPTION AND GEOMETRY OF THE SIMULATED HYDROCYCLONE

The dimensions of the 102 mm Bradley hydrocyclone used in the numerical simulation work are show in the Figure 1. It was considered a 0.0045 mm wall roughness.

## 2.3. MESHING SCHEME

The present computational model is based on a 3D geometry. An unstructured grid with tetrahedral elements was used. This elements permit to fit into small acute angles in the geometry. A grid independence study was carried out with several mesh densities varying from 100,000 to 300,000 elements. Figure 2 shows the mesh over hydrocyclone with 228,219 computational cells, which was considered optimal for good predictions and reasonable computational time for simulations. The entire mesh was generated using the ANSYS CFX® 5.0.

## 2.4. SIMULATION

The simulations carried out on the hydrocyclone were assumed to be operating with water, oil and sand. A cartesian coordinate system was used for the numerical simulations. Multiphase flow simulation was carried out in steady-state and turbulent regimes by using a 3D double-precision. The models based on eqns (1-2-5-6) are implemented in the commercial CFD code ANSYS CFX® 11.0.

A boundary condition prescribed as inlet velocity (20 m/s) was applied at the inlet of the hydrocyclone. In the overflow and underflow we use boundary condition of prescribed outlet pressure (101.3 kPa). The feed oil volume fraction was set to 0.2, the feed sand volume fractions were 0.01, 0.05, 0.10, 0.15 and 0.20, while the feed water volume fraction was determinate by $(1 - f_s - f_o)$. The wall boundary conditions used in this study were non slip to water and oil phases and free slip to solid phase (sand).

Besides, the oil droplet size was assumed equal to 100 μm and 10 μm to sand particle size. The physical properties of the phases (water, oil and sand) used in the simulations are illustrated in Table 1. A convergence criterion of residual type (RMS) $10^{-6}$ was adopted.

Table 1: Physical properties of water, heavy oil and sand

| Properties | Value |
|---|---|
| $\rho$ (heavy oil) | 963.6 (kg/m$^3$) |
| $\mu$ (heavy oil) | 2.0 (Pa.s) |
| $\rho$ (water) | 997.0 (kg/m$^3$) |
| $\mu$ (water) | 0.0008899 (Pa.s) |
| $\rho$ (sand) | 2,780 (kg/m$^3$) |

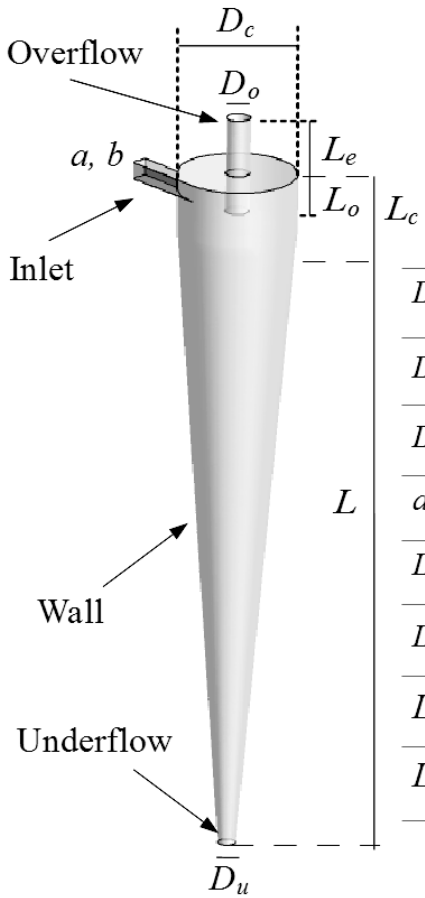


| | | |
|---|---|---|
| $D_c$ | 102.0 | mm |
| $D_o$ | 20.4; 30.6; 36.7 | mm |
| $D_u$ | 24.4 | mm |
| $a, b$ | 14.7 | mm |
| $L$ | 550.8 | mm |
| $L_o$ | 19.4 | mm |
| $L_e$ | 50.0 | mm |
| $L_c$ | 51.0 | mm |

Figure 1: Dimensions of hydrocyclone.

## 3. RESULTS AND DISCUSSION

### 3.1. EFFECT OF SOLID CONCENTRATION IN THE INLET SECTION ON THE SEPARATION PROCESS

To illustrate the numerical results of the approach described in the previous section, the streamline of sand, oil and water are shown in Figures 3, 4 and 5, respectively. By analyzing the figures we can observe that, by increasing the inlet sand concentration (or volume fraction), the intensity of the angular momentum increases, especially to the dispersed phase

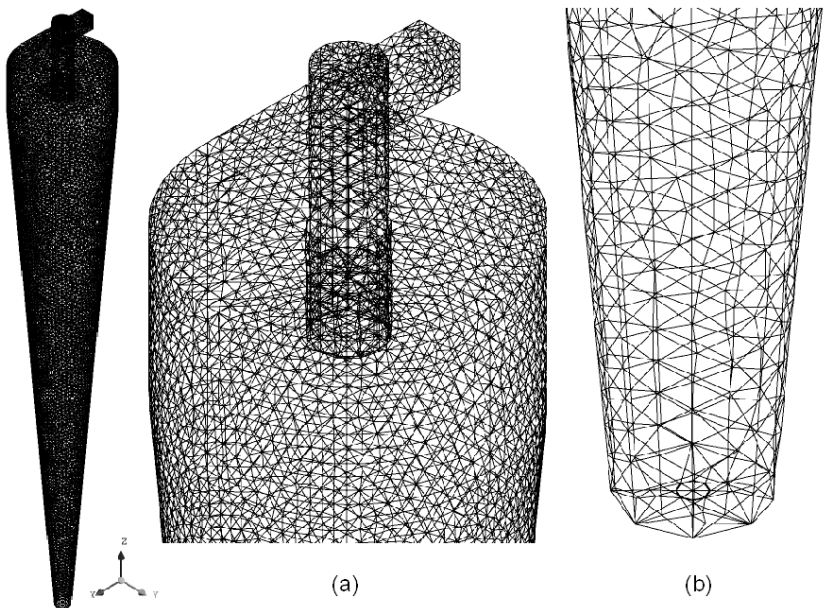


Figure 2: Details of the numerical grid.

(sand). It can be observed yet that water and oil streamlines are practically independents of inlet sand concentration of the mixture. We can observe that the oil migrates to the centre of the hydrocyclone (Figure 4) and the sand is forced towards the wall (Figure 3), moreover, the streamlines for water has two streams: one upward in the center of the hydrocyclone and the second downward near the hydrocyclone wall (Figure 5). This behavior can be explained basically by the external and internal fields of acceleration (gravity and centrifugal forces) and by the drag exerted by the flow. Features of these streamlines such as the reverse flow core and vortex are factors contributing to the pressure drop and effectiveness of the hydrocyclone. By increasing the solid particles concentration into the hydrocyclone we have more friction losses between the solid particles and the hydrocyclone wall.

Figure 6 shows the solids concentration distribution in the *yz* plane for $x = 0$. Note that there is a higher concentration of solid particles near the wall of the hydrocyclone, especially in the conic section. This leads to a variation in pressure drop across the hydrocyclone, as shown in Figure 7. This phenomenon is a consequence of the centrifugal and drag forces acting on the solid particle, which can increase when the solid concentration in the inlet section of the hydrocyclone increases. In addition, a dense flow is characterized by high collision frequencies between particles, and hence their motion is dominantly influenced by particle–particle collisions. Moreover, according to Sommerfeld [19] the interactions between the fluid and particles are of minor importance. This situation can be seen in Figure 8, which depicts the distribution of oil concentration on the *yz* plane. We can observe that the oil concentration distribution practically does not change with the increase of solid concentration in the inlet section of hydrocyclone.

An increase in sand content from 1 to 20% is seen to affect the separation efficiency of the hydrocyclone which can be calculated by the following equations:

$$E_{underflow} = 100 \cdot \frac{\omega_u}{\omega_i} \tag{17}$$


Figure 3: Streamlines of solid phase (sand) to different inlet sand volumetric fraction: (a) 0.01; (b) 0.05; (c) 0.10; (d) 0.15; (e) 0.20.

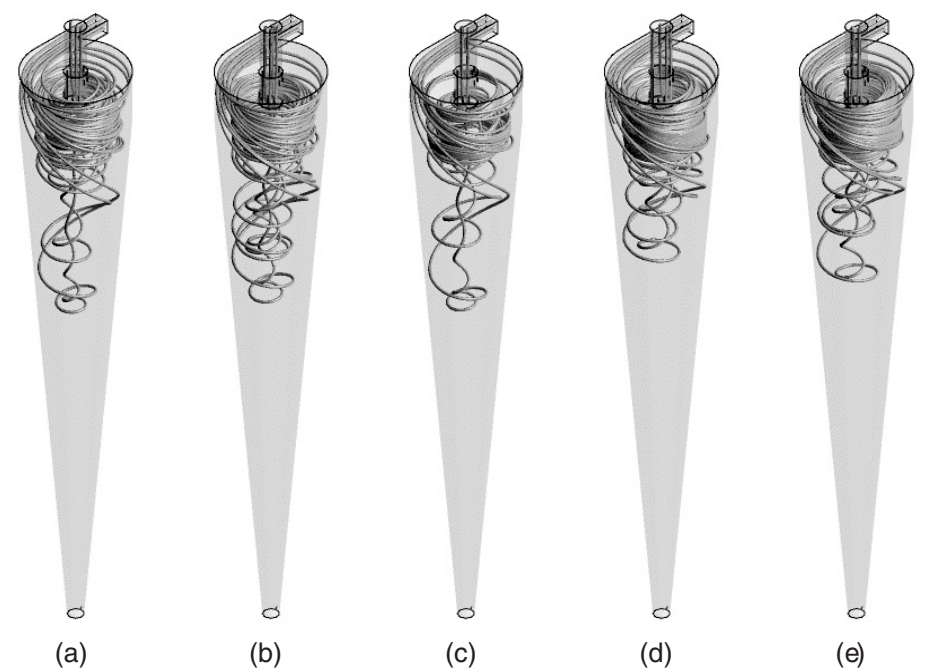


Figure 4: Streamlines of oil phase to different inlet sand volumetric fraction: (a) 0.01; (b) 0.05; (c) 0.10; (d) 0.15; (e) 0.20.

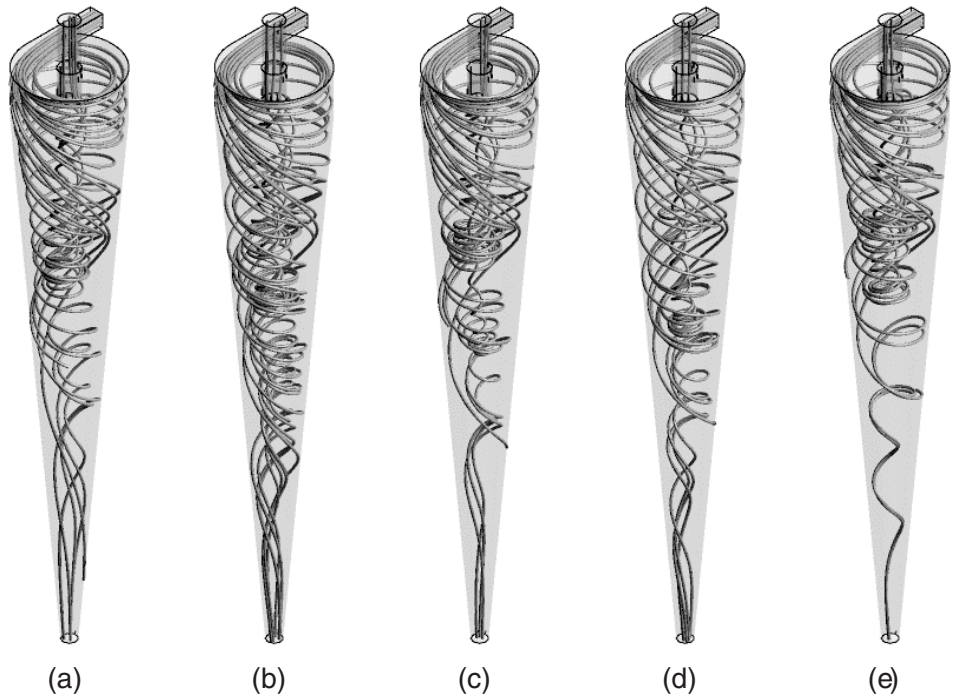


Figure 5: Streamlines of water phase to different inlet sand volumetric fraction: (a) 0.01; (b) 0.05; (c) 0.10; (d) 0.15; (e) 0.20.

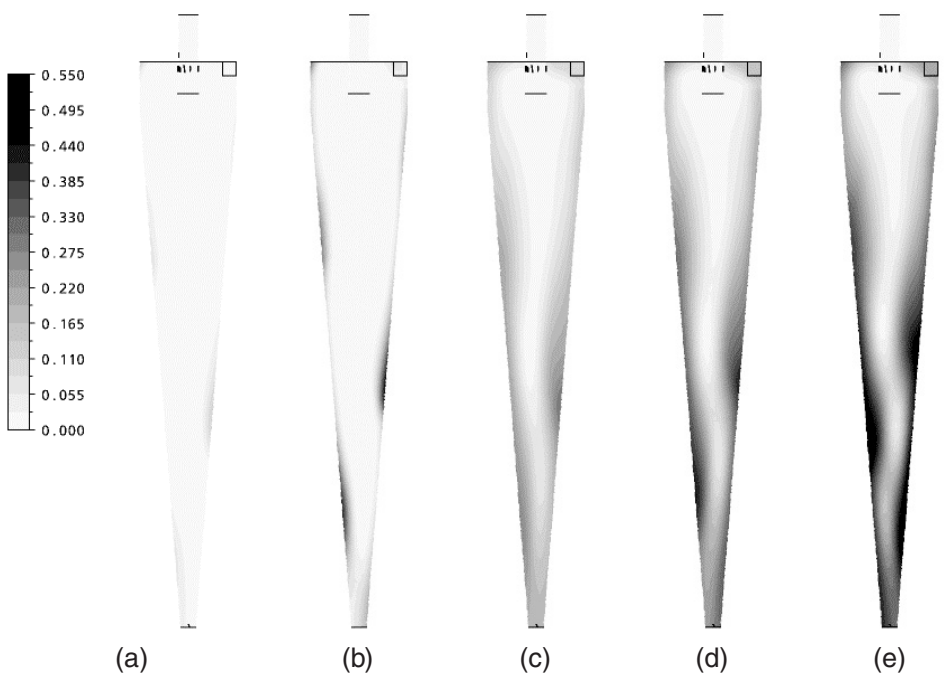


Figure 6: Sand volume fraction fields in the *yz* plane for $x = 0$ to different inlet sand volumetric fraction: (a) 0.01; (b) 0.05; (c) 0.10; (d) 0.15; (e) 0.20.

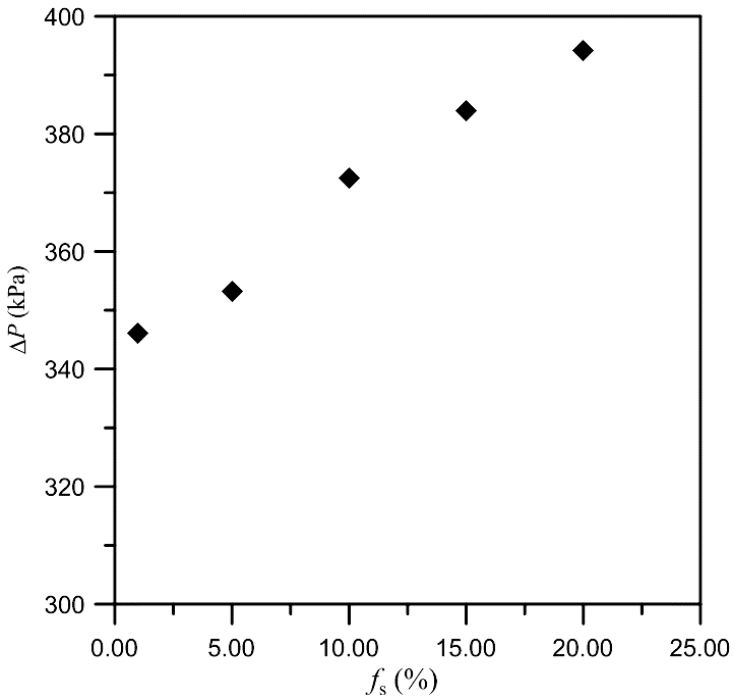


Figure 7: Pressure drop in the hydrocyclone as a function of sand volume fraction in the inlet section.

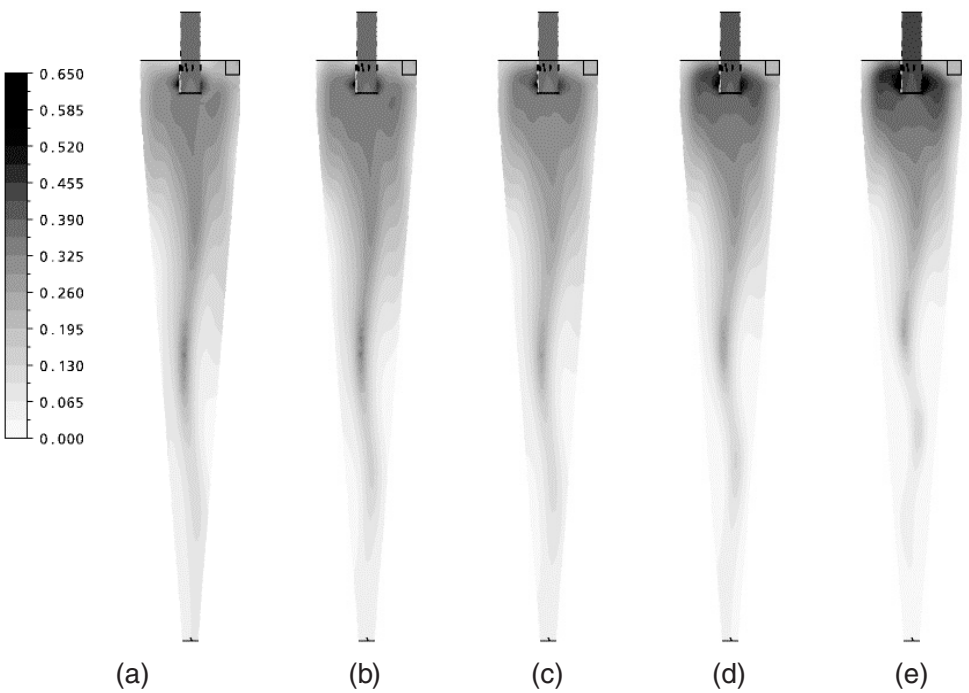


Figure 8: Oil volume fraction fields in the *yz* plane for $x = 0$ to different inlet sand volumetric fraction: (a) 0.01; (b) 0.05; (c) 0.10; (d) 0.15; (e) 0.20.

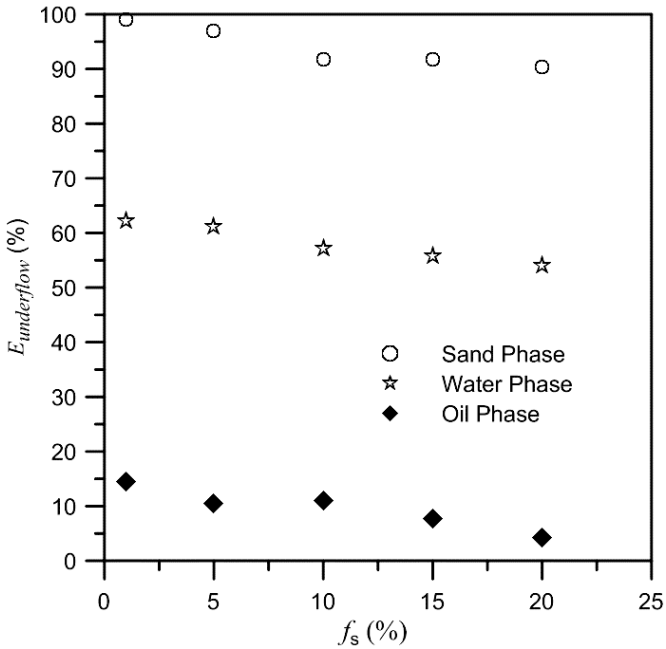


Figure 9: Effects of solid concentration on the hydrocyclone performance (underflow separation efficiency).

$$E_{overflow} = 100 \cdot \frac{\omega_o}{\omega_i} \tag{18}$$

where $\omega_u$, $\omega_o$ and $\omega_i$ are underflow, overflow and inlet mass flow rate (kg/s).

Figure 9 illustrates that the separation efficiency has been influenced by the inlet solid concentration reaching values between 90.3 and 99.12%, while Figure 10 shows that the oil concentration ranged from 87.8 to 98.82%. This represents a drop of 8.86% to solid particle separation efficiency and an increase of 11.02% for oil droplet separation efficiency. Besides, in Figures 9 and 10, we can observe the presence of the continuous phase (water) at both outlets of the hydrocyclone.

## 3.2. EFFECT OF THE VORTEX FINDER DIAMETER ON THE SEPARATION PROCESS

The performance of a hydrocyclone is strongly dependent on its structure and it is always accompanied by some disadvantages, such as unsatisfactory separation and high energy loss. These disadvantages are due to the multiphase flow characteristics inside the hydrocyclone. In this sense, the effect of the hydrocyclone overflow diameter on the oil/water/sand separation was examined. All simulations were realized assuming the following volume fraction: 0.05 for sand; 0.75 for oil, and 0.20 for water.

Figures 11, 12 and 13 show the streamlines of sand, oil and water phases, respectively. These results illustrate a strong dependence of the flow behavior with increasing hydrocyclone overflow diameter. Note also that the behavior of flow lines for sand indicate a greater dependence than the other phases, as expected. Results obtained by Belaidi and Thew [20] related to separation in a de-oiling hydrocyclone shows that the hydrocyclone overflow diameter is a very critical parameter, in terms of control and separation.

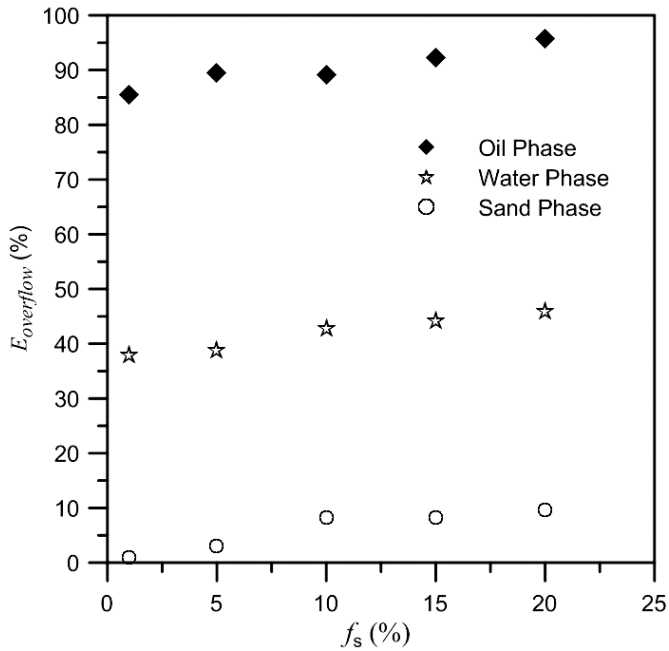


Figure 10: Effects of solid concentration on the hydrocyclone performance (overflow separation efficiency).

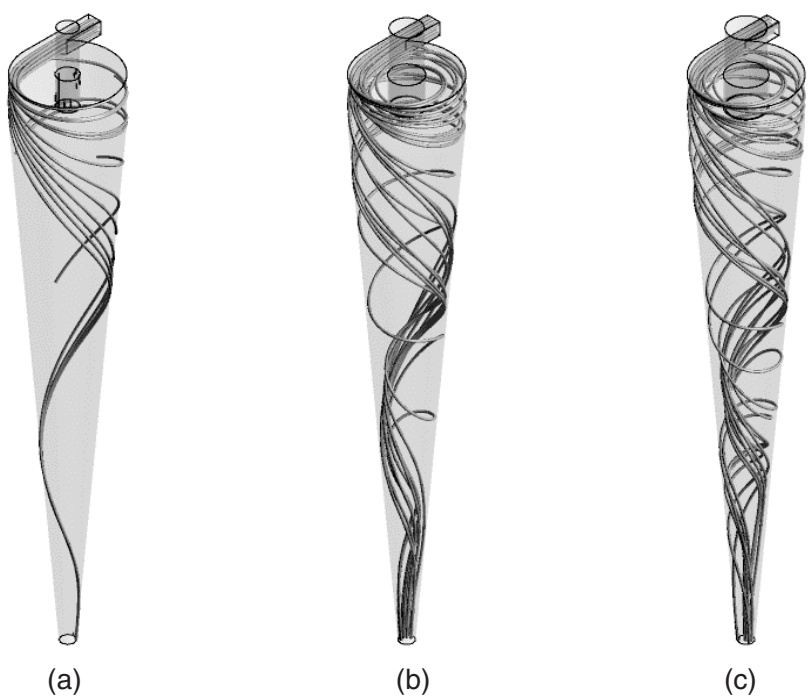


Figure 11: Streamlines of sand phase inside the hydrocyclone with different vortex finder diameters ($D_o$): (a) H1 (20.4 mm); (b) H2 (30.6 mm) and (c) H3 (36.72 mm).

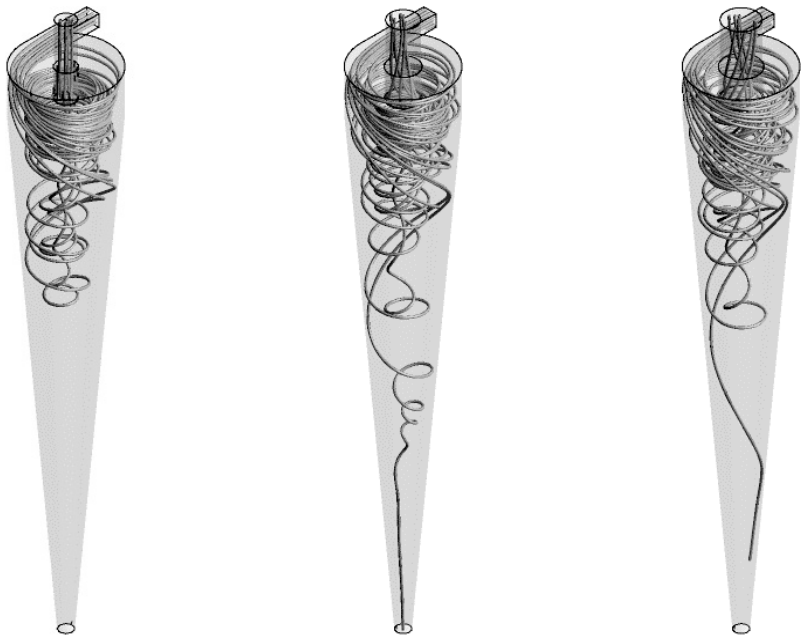


Figure 12: Streamlines of oil phase inside the hydrocyclone with different vortex finder diameters ($D_o$): (a) H1 (20.4 mm); (b) H2 (30.6 mm) and (c) H3 (36.72 mm).

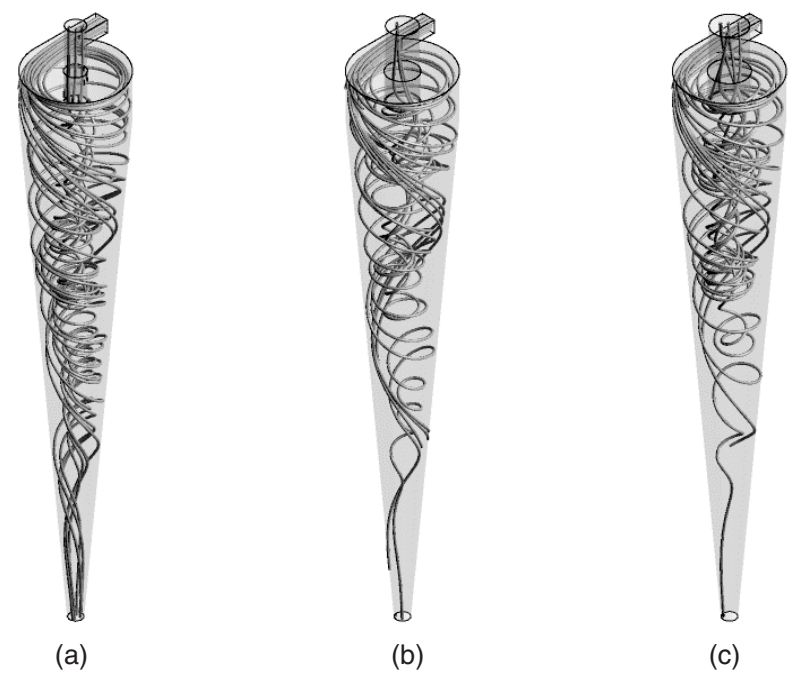


Figure 13: Streamlines of water phase inside the hydrocyclone with different vortex finder diameters ($D_o$): (a) H1 (20.4 mm); (b) H2 (30.6 mm) and (c) H3 (36.72 mm).

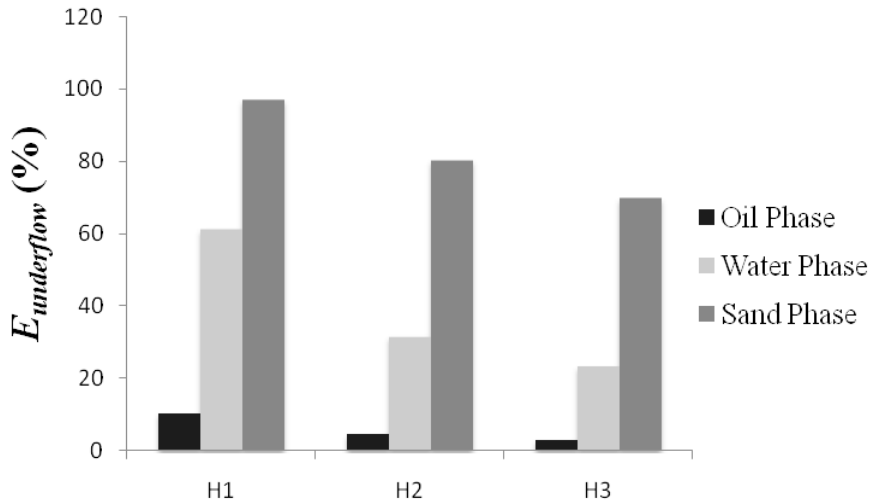


Figure 14: Effect of the hydrocyclone overflow diameter on the underflow separation efficiency.

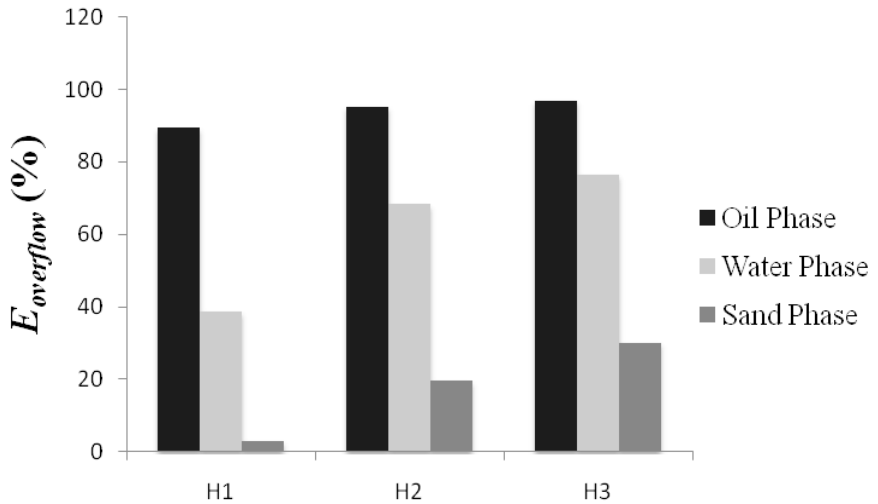


Figure 15: Effect of the hydrocyclone overflow diameter on the overflow separation efficiency.

Figures 14 and 15 illustrate the underflow and overflow separation efficiency respectively to oil, water and sand phases for three hydrocyclone overflow diameters H1 ($D_o$ = 20.4 mm), H2 ($D_o$ = 30.6 mm), H3 ($D_o$ = 36.7 mm). In Figure 14 we can observe that the underflow separation efficiency reduces gradually for all phases. As expected, practically all solid particles are present in this outlet section, due to its higher density than the other phases. Results of Figure 14 show that increasing the hydrocyclone overflow diameter there is a gradual increase of the separation efficiency of all phases; however, there is an increase in concentrations of sand and water in the overflow outlet which is not an interesting situation for the performance of a hydrocyclone.

## 4. CONCLUSIONS

In concordance with the numerical results, we can conclude in general that:

- The proposed model provides a convenient way to study the effects of the different solid concentrations in the inlet section and different hydrocyclone overflow diameter on the separation performance;
- Swirling flow by hydrocyclone presents a complex dynamic behavior;
- By increasing the inlet solid concentration the pressure drop increase within the hydrocycone;
- The separation efficiency has been influenced by the inlet solid concentration reaching values between 90.3 and 99.12%, while that the oil concentration ranged from 87.8 to 98.82%;
- The separation efficiency of the hydrocyclone increases with the increase of the inlet sand concentration, but showed a significant increase in sand and water in the overflow outlet.
- The numerical results confirm a strong dependence of the flow behavior with increasing hydrocyclone overflow diameter.

## 5. ACKNOWLEDGEMENTS

The authors are grateful to CNPq, FINEP, CT-PETRO, ANP, CAPES, UFCG and JBR Engenharia Ltda (Brazil), for financial support.

## 6. REFERENCES

[1] Farias, F. P. M., Buriti, C. J. O., Lima, W. C. P. B., Farias Neto, S. R. and Lima, A. G. B., Numerical Simulation of the Process for Separating Sand/Water/Oil Heavy in a Hydrocyclone, In: *Congreso de Métodos Numéricos en Ingeniería* (Barcelona, Spain), 2009, Vol. 1, 1–14.

[2] Kharoua, N., Khezzar, L. and Nemouchi, Z., Hydrocyclones for de-oiling Applications - A Review, *Petroleum Science and Technology*, 2010, **28** (7), 738–755.

[3] Farias, F.P.M., *Theorical Study of Thermal Fluid Dynamics in Cyclonic Dryers*, PhD Thesis, Federal University of Campina Grande, Brazil, 2006. (*in Portuguese*)

[4] Kharoua, N., Khezzar, L. and Nemouchi, Z., Computational Fluid Dynamics Study of the Parameters Affecting Oil-Water Hydrocyclone Performance, *Journal of Process Mechanical Engineering*, 2009, **24** (2), 119–128.

[5] Cullivan, J. C., Willians, R. A. and Cross, C. R., Understanding the Hydrocyclone Separator through Computational Fluid Dynamics, *Transactions of the Institution of Chemical Engineers*, 2003, **81**, Part A, 455–466.

[6] Petty, C. A. and Parks, S. M., Flow Structures within Miniature Hydrocyclones, *Minerals Engineering*, 2004, **17** (5), 615–624.

[7] Simões, A. M. B. M., *Numerical Simulation of Computational Fluid Dynamics of the Hydrocyclone Applied in Oil/Water Separation*, Master Thesis, Federal University of Campina Grande, Brazil, 2005. (*in Portuguese*).

[8] Brennan, M. S., Narasimba, M. and Holtham, P. N., Multiphase Modelling of Hydrocyclones - prediction of cut-size, *Minerals Engineering* 2007, **20**, 395–406.

[9] Delgadillo, A.J. and Rajamani, R.K., Exploration of Hydrocyclone Designs using Computational Fluid Dynamics, *International Journal of Mineral Processing*, 2007, **84**, 252–261.

[10] Sripriyaa, R., Kaulaskarb, M.D., Chakrabortyb, S. and Meikapb, B.C., Studies on the Performance of a Hydrocyclone and Modeling for Flow Characterization in Presence and Absence of Air Core, *Chemical Engineering Science*, 2007, **62**, 6391–6402.

[11] Zhao, L., Jiang, M. and Wang, Y., Experimental Study of a Hydrocyclone under Cyclic Flow Conditions for Fine Particle Separation, *Separation and Purification Technology*, 2007, **59** (2), 183–189.

[12] Farias, F. P. M., Farias Neto, S. R., Lima, A. G. B. and Buriti, C. J. O., Performance of the Water/Glycerine Separation by Hydrocyclone, *8th. World Congress on Computational Mechanics (WCCM8)/5th. European Congress on Computational Methods in Applied Sciences and Engineering* (ECCOMAS), 2008, Venice, Italy, Vol. 1, 1–2.

[13] Martínez, L. F., Lavín, A. G., Mahamud, M. M. and Bueno, J. L., Vortex Finder Optimum Length in Hydrocyclone Separation, *Chemical Engineering and Processing: Process Intensification*, 2008, **47** (2), 192–199.

[14] Mousavian, S. M. and Najafi, A. F, Influence of Geometry on Separation Efficiency in a Hydrocyclone, *Archive of Applied Mechanics*, 2008, **79** (5), 395–409.

[15] Wang, B. and Yu, A.B., Numerical Study of the Gas–Liquid–Solid Flow in Hydrocyclones with Different Configuration of Vortex Finder, *Chemical Engineering Journal*, 2008, **135**, 33–42.

[16] Buriti, C. J. O., *Application of the Hydrocyclone on the Separation Process Multiphase Fluid Oil/Water/Sand during Production*, Monography, Federal University of Campina Grande, Brazil, 2009. (*in Portuguese*)

[17] Kraipech, W., Nowakowski, A., Dyakowski, T. and Suksangpanomrung, A., An Investigation of the Effect of the Particle–Fluid and Particle–Particle Interactions on the Flow within a Hydrocyclone, *Chemical Engineering Journal*, 2005, **111** (2–3), 189–197.

[18] ANSYS CFX, User Manual Theory, 2006, USA.

[19] Sommerfeld, M., Validation of a Stochastic Lagrangian Modeling Approach for Inter-Particle Collisions in Homogeneous Isotropic Turbulence, *International Journal of Multiphase Flow*, 2001, **27**, 1829–1858.

[20] Belaidi, A. and Thew, M. T., The Effect of Oil and Gas Content on the Controllability and Separation in a De-oiling Hydrocyclone, *Transactions of the Institution of Chemical Engineers*, 2003, **81** (3), 305–314.